Ligand-to-Diimine/Metal-to-Diimine Charge-Transfer Excited States of [Re(NCS)(CO)$_3$(α-diimine)] (α-diimine = 2,2′-bipyridine, di-^{i}Pr-*N*,*N*-1,4-diazabutadiene). A Spectroscopic and Computational Study

Ana Maria Blanco Rodríguez,[†] Anders Gabrielsson,[†] Majid Motevalli,[†] Pavel Matousek,[‡] Michael Towrie,[‡] Jakub Sebera,[§,⊥] Stanislav Záliš,[*,§] and Antonín Vlček, Jr.[*,†,§]

Department of Chemistry and Centre for Materials Research, Queen Mary, University of London, Mile End Road, London E1 4NS, United Kingdom, Central Laser Facility, CCLRC Rutherford Appleton Laboratory, Chilton, Didcot, Oxfordshire OX11 0QX, United Kingdom, and J. Heyrovský Institute of Physical Chemistry, Academy of Sciences of the Czech Republic, Dolejškova 3, CZ-182 23 Prague, Czech Republic

Received: December 26, 2004; In Final Form: April 27, 2005

Two new complexes *fac*-[Re(NCS)(CO)$_3$(N,N)] (N,N = 2,2′-bipyridine (bpy), di-^{i}Pr-*N*,*N*-1,4-diazabutadiene (^{i}Pr-DAB)) were synthesized and their molecular structures determined by X-ray diffraction. UV−vis absorption, resonance Raman, emission, and picosecond time-resolved IR spectra were measured experimentally and calculated with TD-DFT. A good agreement between experimental and calculated ground- and excited-state spectra is obtained, but only if the solvent (MeCN) is included into calculations and excited state structures are fully optimized at the TD-DFT level. The lowest excited states of the bpy and ^{i}Pr-DAB complexes are assigned by TD-DFT as ^{3}aA′ by comparison of calculated and experimental IR spectra. Excited-state lifetimes of 23 ns and ca. 625 ps were determined for the bpy and DAB complex, respectively, in a fluid solution at room temperature. Biexponential emission decay (1.3, 2.7 μs) observed for [Re(NCS)(CO)$_3$(bpy)] in a 77 K glass indicates the presence of two unequilibrated emissive states. Low-lying electronic transitions and excited states of both complexes have a mixed NCS → N,N ligand-to-ligand and Re → N,N metal-to-ligand charge-transfer character (LLCT/MLCT). It originates in mixing between Re d_π and NCS π characters in high-lying occupied MOs. Experimentally, the LLCT/MLCT mixing in the lowest excited state is manifested by shifting the ν(CO) and ν(NC) IR bands to higher and lower wavenumbers, respectively, upon excitation. Resonant enhancement of both ν(CO) and ν(NC) Raman bands indicates that the same LLCT/MLCT character mixing occurs in the lowest allowed electronic transition.

Introduction

Rhenium(I) carbonyl−polypyridine complexes *fac*-[Re(L)(CO)$_3$(N,N)]$^{n+}$ (N,N = polypyridine or α-diimine) form an important class of photoactive compounds, which find applications ranging from probes and sensors[1−6] to photosensitizers capable of triggering electron transfer in metalloproteins.[7−11] Their photophysical and photochemical behavior depends on the nature of low-lying excited states which, in turn, can be controlled by structural variations of the ligands L and N,N, or by the medium.[12] A strong emission from long-lived excited states, inter- and intramolecular excited-state electron transfer, ligand isomerization, or photochemical Re−L bond homolysis are just a few examples of the diverse photobehavior of *fac*-[Re(L)(CO)$_3$(N,N)]$^{n+}$ complexes.[12−36]

The lowest allowed electronic transitions and excited states of *fac*-[Re(L)(CO)$_3$(N,N)]$^{n+}$ are usually described as Re → N,N metal-to-ligand charge transfer (MLCT), while L → N,N ligand-to-ligand charge-transfer excited states (LLCT or XLCT) can occur in complexes where L is an electron-rich ligand, such as halides.[12,37,38] The MLCT and LLCT characters cannot be clearly distinguished since the occupied Re- and L-based orbitals, in which these transitions originate, mix in the high-lying occupied MOs. The extent of the involvement of the axial ligand L in electronic transitions, that is of the mixing between the MLCT and LLCT characters in low-lying excited states of *fac*-[Re(L)(CO)$_3$(N,N)]$^{n+}$, remains an open question. It has been raised for halide complexes where it is difficult to tackle experimentally because of the lack of observables characterizing the actual state of the halide ligand. Nevertheless, an indirect evidence for an admixture of an LLCT character has been reported. It includes resonance enhancement of a Raman band due to a Re−Br stretching vibration in *fac*-[Re(Br)(CO)$_3$(bis-(*p*Tol)-*N*,*N*′-diaza-1,4-butadiene)],[37] or a pronounced dependence of photophysical properties of *fac*-[Re(X)(CO)$_3$(N,N)]$^{n+}$ and *trans*(*Me*,*X*)-[Ru(Me)(X)(CO)$_2$(N,N)] on the halide ligand (X = Cl, Br, I).[12,38−40] MLCT-LLCT mixing also has been suggested by DFT calculations of [Mn(Br)(CO)$_3$(N,N)][41,42] and by TD-DFT and/or CASSCF/CASPT2 calculations of *trans*(*X*,*X*)-[Ru(X)$_2$(CO)$_2$(N,N)] and *trans*(*Me*,*X*)-[Ru(Me)(X)(CO)$_2$(N,N)].[43−45] However, there are several problems with calculations of halide complexes of low-valent metals such as Re^{I} or Ru^{II}. First, the excited-state characters strongly depend on the computational technique used, with TD-DFT consistently predicting much larger LLCT admixture (that is electron density decrease on L upon excitation) than CASSCF/CASPT2.[43,44]

* Address correspondence to these authors. E-mail: a.vlcek@qmul.ac.uk; zalis@jh-inst.cas.cz.
† Queen Mary, University of London.
‡ CCLRC Rutherford Appleton Laboratory.
§ Academy of Sciences of the Czech Republic.
⊥ Permanent address: Czech Technical University, Faculty of Nuclear Sciences and Physical Engineering, Department of Nuclear Chemistry, Bøehová 7, CZ 115 19 Prague 1, Czech Republic.

10.1021/jp044114z CCC: $30.25
Published on Web 05/20/2005

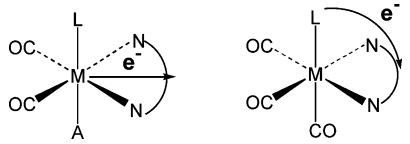

Figure 1. Schematic representation of MLCT (left) and LLCT (right) transitions in *fac*-[Re(L)(CO)$_3$(N,N)]$^{n+}$ complexes.

Moreover, transition energies calculated by TD-DFT in a vacuum are often unrealistically low and the values strongly depend on the functional used.[43,44] Despite these difficulties, the rich photochemical and photophysical behavior of *fac*-[Re(L)(CO)$_3$(N,N)]$^{n+}$ and their wide applicability command the necessity of a correct and deep understanding of their excited-state character and appropriate theoretical description.

Herein, we have approached the problem of MLCT-LLCT mixing by employing a triatomic electron-rich ligand NCS^-, instead of the customary halide. LLCT and MLCT contributions to the lowest excited state can be assessed by monitoring the changes of NCS and CO stretching frequencies upon excitation, respectively, using picosecond time-resolved IR spectroscopy. Resonance enhancement of the corresponding Raman bands provides similar information on the lowest allowed electronic transition. To this effect, we have synthesized two new complexes *fac*-[Re(NCS)(CO)$_3$(N,N)] (N,N = bpy, di-^{i}Pr-*N*,*N*′-1,4-diazabutadiene = ^{i}Pr-DAB). A detailed insight into their excited-state characters and dynamics was achieved by combining spectroscopic and photophysical experiments with quantum chemical calculations, which included the solvent and optimization of the structures of low-lying triplet excited states on a TD-DFT level.

Experimental Section

Materials. All spectroscopic measurements we carried out in solvents of spectroscopic quality, obtained from Aldrich. The product purity was checked by IR spectra in the ν(CO) region, NMR, mass spectroscopy and thin-layer chromatography.

[Re(NCS)(CO)$_3$(bpy)]. [Re(CF_3SO_3)(CO)$_3$(bpy)][46] (0.35 g, 0.61 mmol) was refluxed with [Bu_4N]NCS (0.24 g, 1.3 molar equiv) in dry THF under inert atmosphere for 3 h and the completion of the reaction was controlled by IR. The solvent was removed by rotary evaporation after the reaction mixture was cooled to room temperature. The yellow product was purified by flash chromatography (Si 60, CH_2Cl_2). Crystals for structure determination were grown by a slow diffusion of diethyl ether vapors into a concentrated solution of the complex in CH_2Cl_2.

IR (CH_2Cl_2) ν_{NCS} 2098 cm^{-1}, ν_{CO} 2027, 1920 cm^{-1}; ^{1}H NMR (d_6-acetone) δ 7.88 (2H, t, J = 1.2 Hz), 8.42 (2H, t, J = 1.2 Hz), 8.76 (2H, d, J = 8.2 Hz), 9.15 (2H, d, J = 5.4 Hz); ES-MS m/z 485.7, 484.2 [M^+]

[Re(CF_3SO_3)(CO)$_3$(^{i}Pr-DAB)]. [ReCl(CO)$_3$(^{i}Pr-DAB)][47] (1.2 g, 2.69 mmol) was reacted with Ag(CF_3SO_3) (0.89 g, 1.3 molar equiv) in dry THF and under argon atmosphere. The reaction mixture was heated for 3 h and the completion of the reaction was controlled by IR. After the solution was cooled to room temperature, the precipitate was filtered off and washed with ether and with petroleum spirits. The solvent from the filtrate was removed to produce a dark red oil, [Re(CF_3SO_3)(CO)$_3$(^{i}Pr-DAB)].

IR (CH_2Cl_2) ν_{CO} 2039, 1940, 1923 cm^{-1}.

[Re(NCS)(CO)$_3$(^{i}Pr-DAB)]. The oily [Re(CF_3SO_3)(CO)$_3$(^{i}Pr-DAB)] made in the preceding step was reacted with [Bu_4N]NCS (1.3 molar equiv) in dry THF under inert atmosphere. The reaction mixture was heated for 3 h followed by solvent removal by rotary evaporation. The dark red oil obtained was purified by flash chromatography (Si 60, CH_2Cl_2/MeOH (95/5)). The product was dried under vacuum. Crystals for structure determination were grown by a slow diffusion of diethyl ether vapors into a concentrated solution of the complex in CH_2Cl_2.

IR (CH_2Cl_2) ν_{NCS} 2100 cm^{-1}, ν_{CO} 2027, 1918 cm^{-1}; ^{1}H NMR (d_6-acetone) δ 1.48 (12H, dd, J = 6.3 Hz, DAB CH_3), 4.32 (2H, sept, J = 6.3 Hz, DAB CH_2), 9.00 (2H, s, NH); ES-MS m/z 469.8, 467.9 [M^+]

Instrumentation. X-ray data on [Re(NCS)(CO)$_3$(^{i}Pr-DAB)] were recorded at room temperature on a CAD4 diffractometer fitted with a low-temperature device, operating in the $\omega/2\theta$ scan mode. The structures were solved by standard heavy atom techniques,[48] and refined by least-squares fits[48] on F^2. Data on [Re(NCS)(CO)$_3$(bpy)] were collected at 120 K with a Nonius Kappa CCD area detector diffractometer mounted at the window of a molybdenum rotating anode (50 KV, 90 mA, λ = 0.71069 Å). The crystal-to-detector distance was 30 mm and ϕ and Ω scans (2.0° increments, 12 s exposure time) were carried out to fill the Ewald sphere. The structure was solved by the heavy-atom method and refined anisotropically (non-hydrogen atoms, except C27) by full-matrix least-squares on F^2. The hydrogen atoms were calculated geometrically and refined with a riding model. Refinement details, as well as a full list of atomic coordinates, bond lengths, and angles are available in the Supporting Information. CIF data has been deposited at the CCDC, under the deposition numbers 257965 and 257966.

Time-resolved IR measurements used the equipment and procedures described in detail previously.[22,49−52] In short, the sample solutions were excited (pumped) at 400 or 470 nm, using frequency-doubled Ti:sapphire laser pulses or an OPA output, respectively. The duration (fwhm) of the pump pulses was ∼150 fs. TRIR spectra were probed with IR (∼150 fs) pulses obtained by difference-frequency generation. The IR probe pulses cover a spectral range ∼200 cm^{-1} wide. The sample solutions were flowed through a 0.5 mm CaF_2 IR cell, which was rastering in two dimensions. The spectral bands observed in TRIR spectra were fitted by Lorentzian function to determine accurately their center positions and shapes. All spectral and kinetic fitting procedures were performed with Microcal Origin 7 software. The spectra are shown from 2 ps onward, when the early coherence effects have subsided.

The ground-state resonance Raman spectrum of strongly emissive [Re(NCS)(CO)$_3$(bpy)] was measured from a MeCN solution flowing through a 0.5 mm diameter open jet, using 400 nm laser pulses of a 2 ps duration. Raman scattering was collected during a 4 ps interval determined by a synchronized opening of an optical Kerr gate and it was, thereby, separated from the long-lived interfering emission.[49,50,52,53] Resonance Raman spectra of [Re(NCS)(CO)$_3$(^{i}Pr-DAB)] were collected from a KNO_3 pellet with the Jobin-Yvon XY spectrometer and stationary Ar^+-ion laser excitation at 514.5, 488, or 454 nm.

Room temperature time correlated single photon counting (TCSPC) measurements were performed with a PicoQuant Spectrometer equipped with a microchannel plate photomultiplier detector. The sample was excited at 375 nm with IBH nanoLED. Data were analyzed with IB Datastation2 software. An Edinburgh Instruments FS/FL 900 spectrometer, equipped with a microchannel plate photomultiplier detector, 405 nm diode laser, EdF900 software, and an Oxford Instrument cryostat was employed for the low-temperature (77 K) TCSPC studies.

Quantum Chemical Calculations. Electronic structures of all systems examined were calculated by density functional theory (DFT) methods with the Gaussian 03[54] and Turbo-

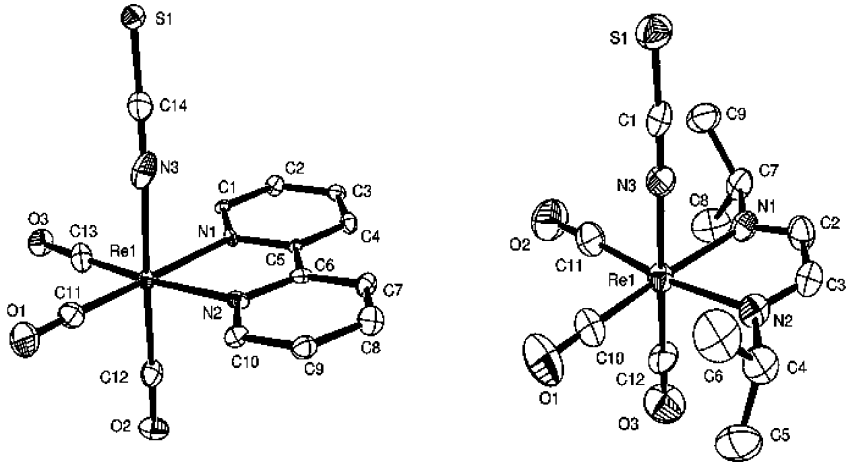

Figure 2. ORTEP diagrams of *fac*-[Re(NCS)(CO)$_3$(bpy)] (left) and *fac*-[Re(NCS)(CO)$_3$(^{i}Pr-DAB)] (right), showing 40% probability ellipsoids. Structures were determined at 120 K and a room temperature, respectively.

mole[55,56] program packages. Low-lying excited states of the closed shell complexes were calculated with time-dependent DFT (TD-DFT). Calculations of vibrational frequencies were performed at TD-DFT optimized geometries corresponding to the functional and basis set used. Triplet excited-state structures were optimized at the TD-DFT level[57] and their IR spectra modeled with use of the Turbomole program package. The conductor-like screening model[58] (COSMO, Turbomole) or the conductor-like polarizable continuum model[59] (CPCM, G03) were used for modeling the solvent influence. Difference density plots were prepared with use of the GaussView software. UV−vis absorption spectra were simulated with the GaussSum[60] software. All transitions calculated in the energy range investigates were included. Gaussian shapes of the absorption bands were assumed. The fwhm value of 0.4 eV used corresponds to typical experimental bandwidths of MLCT bands.[61,62] Band areas are proportional to calculated oscillator strengths.

For geometry optimization, either 6-31G* polarized double-ζ basis sets[63](G03) or the same quality SVP basis (Turbomole) for H, C, N, O, and S atoms together with quasirelativistic effective core pseudopotentials and the corresponding optimized set of basis functions for Re[64] were used. G03 TD-DFT employed cc-pvdz correlation consistent polarized valence double-ζ basis sets[65] for H, C, N, O, and S. Either the hybrid Becke's three-parameter functional with the Lee, Yang, and Parr correlation functional (B3LYP)[66] (G98/B3LYP) or the hybrid functional using Perdew, Burke, and Ernzerhof[67] exchange and correlation functional with 25% HF exchange (PBE1PBE) were used. The geometry optimizations and calculations in solution were carried out without any symmetry restriction. The approximate C_s symmetry is used for the description of the spectra and molecular orbitals. [Re(NCS)(CO)$_3$(Me-DAB)] was calculated as a model for the experimentally studied [Re(NCS)(CO)$_3$(^{i}Pr-DAB)]. It was shown[68] that such a model qualitatively well reproduces spectral properties; nevertheless the absolute values of calculated spectral parameters are influenced by this simplification.

Results and Discussion

Molecular Structure. ORTEP diagrams of *fac*-[Re(NCS)(CO)$_3$(bpy)] and *fac*-[Re(NCS)(CO)$_3$(^{i}Pr-DAB)] are shown in Figure 2 and the selected bond lengths and angles are summarized in Table 1, together with the calculated values. All the structural data are collected in the Supporting Information. [Re(NCS)(CO)$_3$(bpy)] has two molecules in the asymmetric unit, which is shown in Figure 1 of the Supporting Information. The X-ray structures clearly prove that the NCS ligand is coordinated to Re by the nitrogen atom. Bond distances and angles around the Re center are typical for [Re(L)(CO)$_3$(N,N)]$^{n+}$ complexes,[69] with the N(1)−Re−N(2) bite angle being characteristically small. The Re−NCS moiety is bent by 5−10° at the N atom and the Re−N(CS) bond is slightly tilted toward the N,N ligand. The calculated structural parameters agree well with the experimental values. The *fac*-Re(CO)$_3$ unit is a nearly regular trigonal pyramid with ∼90° angles between the CO ligands. The prefix *fac* will be omitted hereafter for brevity.

TABLE 1: Selected Experimental and DFT/B3LYP Calculated Bond Lengths and Angles of [Re(NCS)(CO)$_3$(bpy)] and [Re(NCS)(CO)$_3$(^{i}Pr-DAB)]^a

[Re(NCS)(CO)$_3$(bpy)]			[Re(NCS)(CO)$_3$(DAB)]		
	calcd	exptl		calcd^b	exptl
bond lengths, Å					
Re−N1	2.217	2.159	Re−N1	2.185	2.193
Re−N3	2.121	2.129	Re−N3	2.115	2.114
Re−C12	1.952	1.919	Re−C12	1.959	1.915
Re−C13	1.945	1.882	Re−C10	1.961	1.913
N1−C1	1.345	1.373	N2−C4	1.459	1.478
N1−C5	1.359	1.393	N2−C3	1.295	1.275
C5−C6	1.480	1.441	C3−C2	1.450	1.451
N3−C14	1.186	1.160	N3−C1	1.187	1.167
C14−S1	1.622	1.633	C1−S1	1.619	1.622
C12−O2	1.163	1.151	C12−O3	1.162	1.148
C11−O1	1.160	1.186	C10−O1	1.157	1.139
bond angles, deg					
C12−Re−N3	174.5	176.8	C12−Re−N3	177.7	177.8
C11−Re−C13	90.1	88.2	C11−Re−C10	91.7	86.6
C11−Re−N2	97.8	98.6	C10−Re−N2	97.1	100.4
N1−Re−N2	74.1	74.8	N1−Re−N2	73.9	73.6
N3−Re−N2	82.9	85.2	N3−Re−N2	84.6	84.9
Re−N3−C14	177.5	175.4	Re−N3−C1	176.5	169.6
N3−C14−S1	179.3	177.9	N3−C1−S1	179.2	176.6

^{a} Experimental bond lengths of symmetry-linked bonds are averaged. ^{b} Calculated for [Re(NCS)(CO)$_3$(Me-DAB)].

Electronic Structures. The energies and compositions of frontier Kohn−Sham molecular orbitals calculated by DFT for both molecules in MeCN solutions are summarized in Tables 2 and 3. A qualitative MO diagram and shapes of the spectroscopically relevant MOs are shown in Figure 3.

The two highest occupied MOs of both complexes have a mixed Re/NCS character. They are essentially Re−NCS π-antibonding. The LUMO is a predominantly π* antibonding orbital of the N,N ligand, with a small Re contribution. Both

TABLE 2: DFT G03/PBE1PBE/CPCM (MeCN) Calculated One-Electron Energies and Compositions of Selected Highest Occupied and Lowest Unoccupied Molecular Orbitals of [Re(NCS)(CO)$_3$(bpy)] in MeCN, Expressed in Terms of Composing Fragments

MO	*E*, eV	prevailing character	Re	CO_{ax}	CO_{eq}	NCS	bpy
unoccupied							
35a″	−0.93	Re + CO	28	11	40	5	21
34a″	−1.28	π bpy	10	5	2	0	87
53a′	−1.47	π bpy	4	0	1	0	95
52a′	−2.46	π bpy	13	0	2	0	85
occupied							
33a″	−6.18	NCS + Re	28	4	8	57	2
51a′	−6.23	NCS + Re	24	4	7	62	3
32a″	−7.04	Re	66	0	24	2	8
50a′	−7.24	Re + NCS	36	4	8	42	9
49a′	−7.30	Re + NCS	40	5	10	37	9
31a″	−7.57	π bpy	3	0	0	0	96

TABLE 3: DFT G03/PBE1PBE/CPCM (MeCN) Calculated One-Electron Energies and Compositions of Selected Highest Occupied and Lowest Unoccupied Molecular Orbitals of [Re(NCS)(CO)$_3$(Me-DAB)] in MeCN, Expressed in Terms of Composing Fragments

MO	*E*, eV	prevailing character	Re	CO_{ax}	CO_{eq}	NCS	Me-DAB
unoccupied							
44a′	−0.60	CO + Re	19	37	36	4	4
25a″	−0.97	CO + Re	24	18	47	6	6
43a′	−3.02	π* DAB	6	1	5	1	87
occupied							
24a″	−6.22	NCS + Re	26	8	6	59	2
42a′	−6.29	NCS	21	6	4	65	3
23a″	−7.10	Re	67	0	29	0	3
41a′	−7.33	Re + NCS	36	7	8	42	8
40a′	−7.46	Re + NCS	42	7	8	36	7
22a″	−9.07	π DAB	4	1	0	4	91

LUMO+1 and LUMO+2 are predominantly π*(bpy) for [Re(NCS)(CO)$_3$(bpy)] and π*(CO) for [Re(NCS)(CO)$_3$(Me-DAB)]. Inclusion of the solvent into the calculation modifies the MO compositions, decreasing the NCS and increasing the Re participations in the HOMO and HOMO−1. (MO compositions in a vacuum are summarized in Tables 1 and 2 of the Supporting Information.)

Electronic Transitions. Shown in Figure 4 are the experimental and calculated UV−vis spectra. The lowest absorption band is strongly solvatochromic. For bpy, its maximum shifts from 375 to 399 and 420 nm on changing the solvent from MeCN to CH_2Cl_2 and toluene, respectively. The lowest band of the ^{i}Pr-DAB complex occurs in the same solvents at 428, 468, and 483 nm, respectively. TD-DFT calculations reproduce well the experimental absorption spectra in MeCN and the trend in solvatochromism(see Figure 4 and Tables 4 and 5). The lowest absorption band of both complexes is assigned to the $a^1A' \rightarrow b^1A'$ transition, which originates in an almost pure HOMO−1 → LUMO excitation. Because of a large admixture of an NCS π orbital into HOMO−1, this transition can be viewed as mixed (NCS → N,N)/(Re → N,N) LLCT/MLCT. This assignment is also supported by the solvatochromism, which is typical for charge-transfer transitions.[12,38,70,71]

The best agreement with the experimental spectra was obtained by using the PBE1PBE functional in conjunction with the CPCM solvent model in MeCN. Other functionals such as B3LYP and BP86 underestimate the LLCT/MLCT transition energies, shifting the allowed $a^1A' \rightarrow b^1A'$ transition down to 2.26 eV (549 nm) and 2.03 eV (611 nm), respectively, as calculated for N,N = bpy in MeCN. Neglecting the solvent in the calculation results in unrealistically low transition energies. For example, TD-DFT PBE1PBE/vacuum calculates the $a^1A' \rightarrow b^1A'$ transition at 1.61 eV, that is 1.32 eV lower than in MeCN. It follows from Figure 4 that CPCM provides the best results for the polar MeCN solvent, where the calculated transition energies are only slightly underestimated. The calculations exaggerate the solvatochromism effect, producing too low transition energies for low-polarity CH_2Cl_2 and toluene.

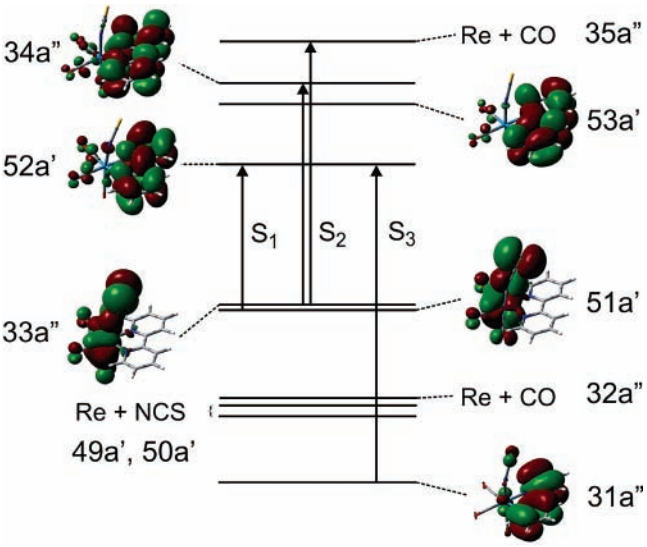

Figure 3. Qualitative MO diagram and shapes of the spectroscopically relevant molecular orbitals. The orbital labels correspond to those in Table 2. The vertical arrows labeled S_1, S_2, and S_3 show the principal excitations involved in the spectroscopically important singlet transitions to the states b^1A', e^1A', and e^1A'', respectively, see Table 4.

The assignment of the lowest allowed transition as LLCT/MLCT is experimentally supported by resonance Raman spectra (rR). The spectrum of the strongly emissive [Re(NCS)(CO)$_3$(bpy)] (Figure 5) was measured with 400 nm laser pulse excitation. It shows weak resonantly enhanced bands at 2098 and 2030 cm^{-1}. These bands are seen also in the FTIR spectrum (Figure 7). The 2038 cm^{-1} corresponds to the in-phase A′(1) ν(CO) vibration, characteristic of *fac*-Re(CO)$_3$ complexes. The band at 2098 cm^{-1} is attributed to the ν(NC) vibration of the NCS ligand by comparison with the spectra of other transition metal complexes with the *N*-coordinated NCS ligand.[72] The rR spectrum shows also bands at 1561, 1490, 1312, 1180, 1022, and 731 cm^{-1}, due to vibrations of the bpy ligand. They are very similar to those observed[73] in the spectrum of [Re(Cl)(CO)$_3$(bpy)] and signify that the resonant electronic transition involves charge transfer to the bpy ligand. The rR spectrum of [Re(NCS)(CO)$_3$(^{i}Pr-DAB)] was measured from a KNO_3 pellet, Figure 6. Intensities of all bands, measured relative to the KNO_3 band at 1051 cm^{-1}, increase when the excitation wavelength is changed from 514.5 to 488 and 457.9 nm toward the maximum of the lowest absorption band, demonstrating the resonance enhancement. The spectrum shows an intense band at 1566 cm^{-1}, which originates in a DAB ν(C═N) vibration, coupled with ν(N−^{i}Pr),[68,74] and bands at 2030 and 2098 cm^{-1}, due to A′(1) ν(CO) and ν(NC), respectively. (See Figure 8 for comparison with FTIR.) Resonance enhancement of the A′(1) ν(CO) band, seen for both complexes, indicates a MLCT character of the resonant transition.[71,75] Simultaneous enhancement of the ν(NC) band shows that bonding within the NCS ligand is affected as well. It follows that the electron density is removed from the whole Re(NCS)(CO)$_3$ moiety, in line with the proposed mixed NCS → dimine LLCT/Re → diimine MLCT character of the resonant transition.

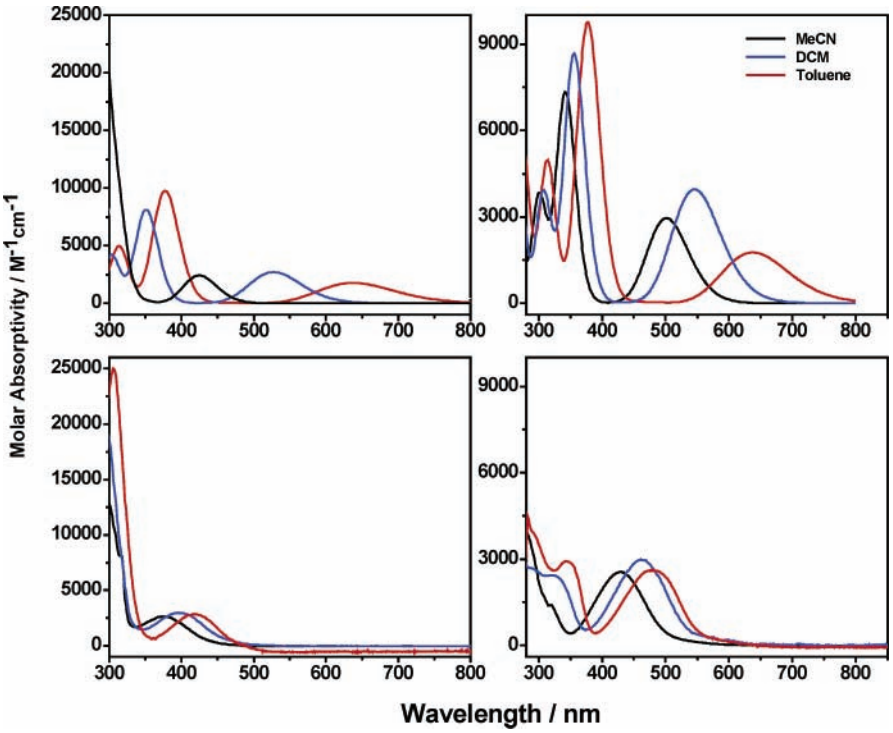

Figure 4. UV−vis absorption spectra of [Re(NCS)(CO)$_3$(bpy)] (left) and [Re(NCS)(CO)$_3$(^{i}Pr-DAB)] (right). Experimental spectra are shown at the bottom, simulated at the top. Spectra are shown in MeCN (black), dichloromethane (blue), and toluene (red). The simulated spectrum of the DAB complex (top right) corresponds to [Re(NCS)(CO)$_3$(Me-DAB)].

TABLE 4: Energies of Low-Lying Singlet Electronic Transitions of [Re(NCS)(CO)$_3$(bpy)] with Oscillator Strength Larger than 0.001 Calculated by TD-DFT G03/PBE1PBE/CPCM (MeCN)

state	main components, %	transition energy, eV (nm)	osc. str.	exptl transition, eV (nm)	molar abs, $M^{-1}\,cm^{-1}$
a^1A''	99 (33a″ → 52a′)	2.83 (438)	0.003		
b^1A'	99 (51a′ → 52a′)	2.93 (424)	0.032	3.31 (375)	2600
b^1A''	98 (32a″ → 52a′)	3.59 (342)	0.003		
c^1A'	88 (51a′ → 53a′); 7 (49a′ → 52a′)	3.95 (314)	0.014		
d^1A'	79 (49a′ → 52a′); 10 (51a′ → 53a′)	3.97 (313)	0.037		
e^1A'	48 (33a″ → 34a″); 31 (33a″ → 35a″)	4.04 (307)	0.069	∼3.91 (317)	
f^1A'	50 (33a″ → 35a″); 38 (33a″ → 34a″)	4.11 (302)	0.029		
e^1A''	67 (31a″ → 52a′); 13 (33a″ → 54a′)	4.35 (286)	0.312	4.23 (293)	14340
f^1A''	66 (33a″ → 54a′); 13 (31a″ → 52a′)	4.36 (285)	0.068		

TABLE 5: Energies of Low-Lying Singlet Electronic Transitions of [Re(NCS)(CO)$_3$(Me-DAB)] with Oscillator Strength Larger than 0.001 Calculated by TD-DFT G03/PBE1PBE/CPCM (MeCN)[a]

state	main components, %	transition energy, eV (nm)	osc. str.	exptl trans., eV (nm)	molar abs, $M^{-1}\,cm^{-1}$
a^1A''	98 (24a″ → 43a′)	2.24 (552)	0.001		
b^1A'	98 (42a′ → 43a′)	2.47 (501)	0.041	2.90 (428)	2500
c^1A'	98 (40a′ → 43a′)	3.62 (342)	0.101		
d^1A'	81 (24a″ → 25a″); 9 (42a′ → 44a′)	4.12 (301)	0.052		
e^1A'	70 (42a′ → 44a′); 17 (24a″ → 26a″)	4.71 (263)	0.056		
e A″	57 (22a″ → 43a′); 20 (24a″ → 45a′)	5.32 (233)	0.146		

[a] Experimental data are for [Re(NCS)(CO)$_3$(^{i}Pr-DAB)].

The low-lying LLCT/MLCT transitions of [Re(NCS)(CO)$_3$-(bpy)] are succeeded at higher energy by a group of close-lying strong transitions which give rise to the intense absorption in the near UV spectral region, Table 4. They include LLCT/MLCT transitions directed to LUMO+1 and LUMO+2, a predominantly MLCT transition $a^1A' \rightarrow d^1A'$, and an intense, predominantly (67%) $\pi\pi^*$ bpy-localized transition $a^1A' \rightarrow e^1A''$. The significant CT contributions are manifested by the solvatochromism, both observed and calculated for the near UV absorption band (Figure 4). For [Re(NCS)(CO)$_3$(^{i}Pr-DAB)], the second allowed transition is MLCT/LLCT $a^1A' \rightarrow c^1A'$, whose energy is underestimated by TD-DFT (Figure 4, Table 5). Nevertheless, its strong solvatochromic shift is reproduced computationally. Re → CO MLCT transitions are calculated to occur at still shorter wavelengths, ≤300 nm.

Triplet Excited States. [Re(NCS)(CO)$_3$(bpy)] shows a weak emission band at 602 nm in a fluid MeOH/EtOH (3/4) solution at room temperature. Emission intensity increases on going to a 77 K glass and the band shifts to 534 nm. Such rigidochromism is characteristic of emission from a state with a substantial CT character: MLCT and/or LLCT.[76−78] The emission decays with a lifetime of 23 ± 1 ns in a MeCN solution at room temperature. It is much longer lived in a MeOH/EtOH (3/4) glass at 77 K, where a biexponential decay was observed:

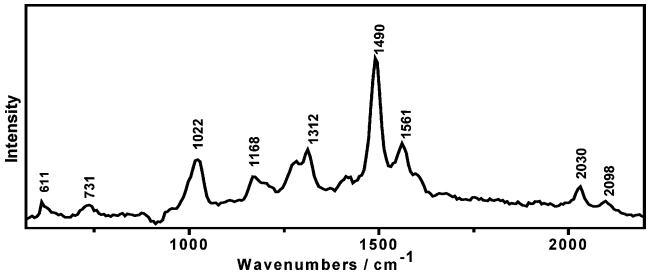

Figure 5. Resonance Raman spectrum of [Re(NCS)(CO)$_3$(bpy)] in MeCN measured using ~2 ps, 400 nm laser pulses synchronized with a 4 ps optical Kerr gate that rejects the long-lived emission. The solvent background and residual emission that passed through the Kerr gate are subtracted.

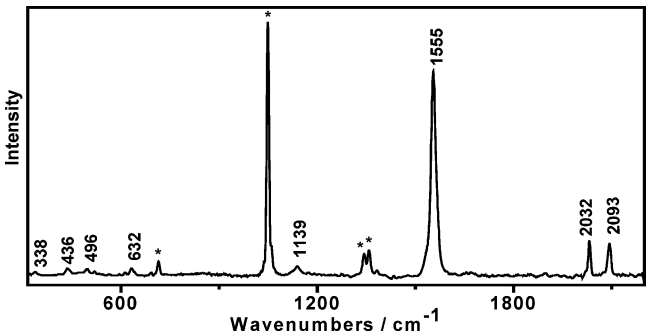

Figure 6. Resonance Raman spectrum of [Re(NCS)(CO)$_3$(^{i}Pr-DAB)] measured in a rotating KNO_3 pellet using continuous laser irradiation at 457.9 nm. Asterisks indicate peaks due to KNO_3.

1.26 ± 0.07 μs (38%) and 2.71 ± 0.10 μs (62%). This behavior suggests the presence of two energetically close-lying emissive excited states, which become equilibrated in a fluid solution at room temperature. [Re(NCS)(CO)$_3$(^{i}Pr-DAB)] is not emissive, presumably due to a very fast nonradiative decay.

TD-DFT was used to optimize the geometry of low-lying triplet excited states and to calculate their energies (Table 6) and vibrational spectra (Tables 7 and 8). The lowest calculated state a^3A'' is composed predominantly of a HOMO → LUMO LMCT/MLCT excitation, and an N,N-localized $\pi \rightarrow \pi^*$ excitation that contributes 15% and 5% for bpy and DAB, respectively. The second state a^3A' originates in the HOMO−1 → LUMO excitation, Table 6. It is the triplet counterpart of the optically populated b^1A' state with the same mixed LLCT/MLCT character. The calculated emission energies of the two lowest triplets of the bpy complex (2.05, 2.22 eV) are very close to the maximum of the emission band, 2.06 eV, as observed in MeCN.

Experimentally, the lowest triplet excited states of both complexes were characterized with picosecond time-resolved IR spectroscopy, TRIR. The TRIR spectra are shown in Figures 7 and 8, together with the ground-state FTIR spectra. Experimental ground- and excited-state IR wavenumbers are summarized in Table 7, together with the values calculated for MeCN solutions. TRIR spectra measured at 2 ps show three fully developed negative bands that correspond to bleached ground-state absorption and four positive bands corresponding to the excited state. Excited-state bands narrow during the first 20 ps, slightly increase in intensity, and shift to higher wavenumbers. This is a typical manifestation of vibrational cooling.[79,80] After the vibrational relaxation is completed, the TRIR spectrum of [Re(NCS)(CO)$_3$(bpy)] does not change until the end of the time interval investigated, that is 1000 ps. For [Re(NCS)(CO)$_3$(^{i}Pr-DAB)], an excited-state lifetime of 625 ps was estimated from the decay of the transient bands and the bleach recovery.

In the ground state, both complexes show a broad band at ca. 1920 cm^{-1}, which encompasses the out-of-phase A′(2) and equatorial A″ ν(CO) vibrations, and bands at 2027 and ~2100 cm^{-1} due to the in-phase A′(1) ν(CO) and ν(NC) vibrations, respectively. The latter two bands are seen also in the rR spectra, compare Figures 5 and 6. Empirically, we assign the excited-state bands of [Re(NCS)(CO)$_3$(bpy)] at 1952, 2002, and 2072 cm^{-1} to upshifted ν(CO) vibrations, as is characteristic for MLCT excitations.[75,79,81−87] The 2041 cm^{-1} band is assigned to the ν(NC) vibration of the NCS ligand. Its downward shift from the ground-state position demonstrates the LLCT contribution to the excitation, which removes electron density from a N═C═S π bonding orbital, weakening the N═C bond and thus decreasing the ν(CO) frequency. The assignment of the 2072 cm^{-1} band as ν(CO) is corroborated by the effect of changing the solvent to less polar CH_2Cl_2, in which this band occurs at 2059 cm^{-1}. Decreasing the solvent polarity diminishes the extent of the charge transfer from the Re(CO)$_3$ unit. This is manifested by a smaller shift of the highest ν(CO) band upon excitation: +32 cm^{-1} in CH_2Cl_2 vs +46 cm^{-1} in MeCN.

Excited-state IR spectra were calculated in an MeCN cavity (COSMO) with TD-DFT optimized excited structures. A very good agreement was achieved between the experimental excited-state spectrum and the vibrational wavenumbers, calculated by TD-DFT for the ^{3}LLCT/MLCT state ^{3}aA′, Table 7. The IR spectrum calculated for the ^{3}aA″ state does not correspond well to the experiment. Hence, we conclude that ^{3}aA′ is the lowest excited state at the actual experimental conditions, although it was calculated as the second lowest state. The calculations provide a deeper insight into the characters of the vibrations. While the ν(CO) and ν(NC) vibrations are well defined in the ground state, they become strongly coupled in the excited state, Table 8. The excited-state vibrations calculated at 2010 and 2038 cm^{-1} belong to an ν(NC) vibration coupled with A′(1) and A′(2) ν(CO) vibration, respectively. The lowest 1952 cm^{-1} vibration is assigned essentially as A′(1) ν(CO). The highest excited-state vibration at 2082 cm^{-1} is ν(CO), in agreement with the empirical assignment. Surprisingly, the TD-DFT calculation shows that this vibration involves the equatorial CO ligands, resembling the A″ ν(CO) vibration of the ground state. (Note that the use of the symmetry labels for excited states is only approximate since the C_s molecular symmetry is lost.)

Excited-state TRIR spectra of [Re(NCS)(CO)$_3$(^{i}Pr-DAB)] show similar features as discussed above for [Re(NCS)(CO)$_3$(bpy)], although the shifts of the IR bands upon excitation are somewhat smaller and the highest vibration is manifested as a ~2068 cm^{-1} shoulder on the most intense 2053 cm^{-1} band, Figure 8 and Table 7. The solvent effect is much weaker than seen for bpy.[88] The IR spectrum calculated for the a^3A'' state agrees satisfactorily with the experimental TRIR, given that the calculation was performed for a model complex with a Me-DAB ligand instead of ^{i}Pr-DAB. Analysis of the calculated vibrations shows that the highest two bands correspond to highly mixed ν(CO) and ν(NC) vibrations, Table 8. The equatorial ν(CO) A″ vibration occurs as the second lowest band (1986 cm^{-1}), at much lower wavenumbers than for bpy.

The assignment of the highest IR band of the a^3A' excited state [Re(NCS)(CO)$_3$(bpy)] to an equatorial A″-like ν(CO) vibration contradicts the usual assignment used for similar complexes, such as [Re(Cl)(CO)$_3$(4,4′-bpy)$_2$] and [Re(Etpy)-(CO)$_3$(bpy)]$^+$, respectively, where the A″ vibration is supposed to give rise to the lowest or second lowest ν(CO) IR band of a

TABLE 6: TD-DFT Calculated (G03/PBE1PBE/CPCM) Lowest Triplet Excitation Energies for [Re(NCS)(CO)$_3$(N,N)] Complexes in MeCN

N,N	state	main components, %	emission energy,[a] eV (nm)	transition energy,[b] eV (nm)
bpy	a^3A''	65 (33a″ → 52a′); 19 (32a″ → 52a′); 15 (31a″ → 52a′)	2.05 (605)	2.75 (451)
	a^3A'	91 (51a′ → 52a′)	2.22 (559)	2.86 (433)
	b^3A''	47 (31a″ → 52a′); 36 (32a″ → 52a′); 16 (33a″ → 52a′)		3.01 (411)
	c^3A'	98 (50a′ → 52a′)		3.53 (351)
Me-DAB	a^3A''	87 (24a″ → 43a′); 8 (23a″ → 43a′); 5 (22a″ → 43a′)		1.83 (676)
	a^3A'	97 (42a′ → 43a′)	1.64 (754)	1.97 (630)
	b^3A''	67 (22a″ → 43a′); 24 (23a″ → 43a′); 8 (24a″ → 43a′)		2.58 (480)
	c^3A'	93 (41a′ → 43a′)		2.72 (455)

[a] Calculated vertical transition at TD-DFT optimized geometry of the given triplet state. [b] Calculated vertical transition at ground-state optimized geometry.

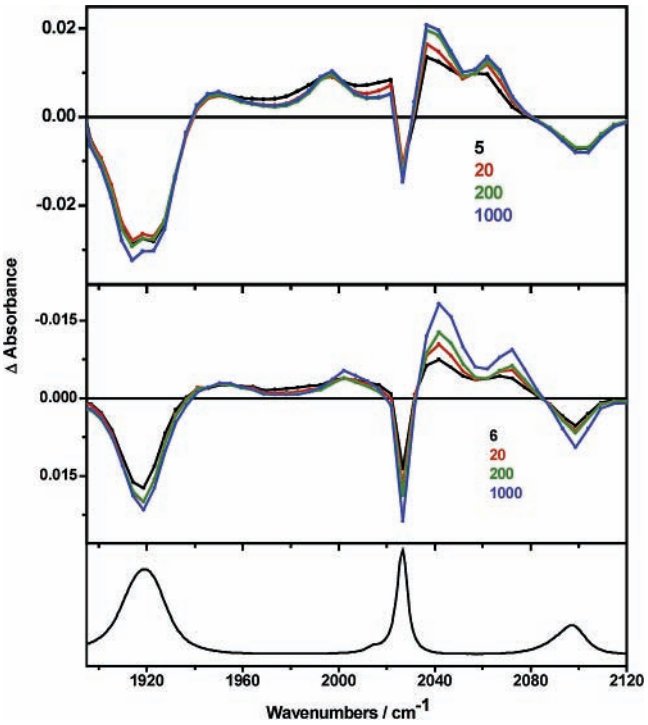

Figure 7. Difference TRIR spectra of [Re(NCS)(CO)$_3$(bpy)] in CH_2Cl_2 (top) and MeCN (bottom) measured after 400 nm, ~150 fs excitation at time delays (ps) specified in the insets. Experimental points are separated by 4−5 cm^{-1}. The ground-state FTIR spectrum is shown in the bottom panel.

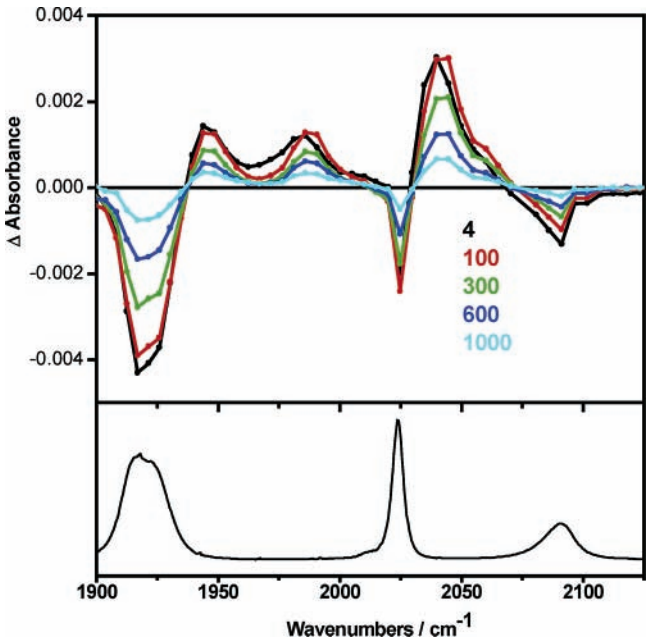

Figure 8. Difference TRIR spectrum of [Re(NCS)(CO)$_3$(^{i}Pr-DAB)] in THF measured after 470 nm, ~150 fs excitation at time delays (ps) specified in the inset. Experimental points are separated by 4−5 cm^{-1}. The ground-state FTIR spectrum is shown in the bottom panel.

^{3}MLCT excited state and the highest band is invariably attributed to the A′(1) ν(CO).[75,85−87] To resolve this discrepancy, we have calculated ν(CO) wavenumbers of the lowest a^3A'' excited state of [Re(Cl)(CO)$_3$(bpy)], which has a predominantly MLCT/LLCT character with a minor $\pi \rightarrow \pi^*$(bpy) intraligand admixture.[62,89] The ν(CO) vibrations are essentially pure, since there are no other vibrations in the same frequency range with which they could couple. The results are shown in Table 9. Again, a good agreement between experimental and calculated wavenumbers was obtained, although the excited-state ν(CO) wavenumbers are somewhat underestimated. The calculated normal coordinates confirm the usual order of excited-state IR ν(CO) bands: A″ < A′(2) < A′(1). Comparison of the results calculated for [Re(NCS)(CO)$_3$(bpy)] and [Re(Cl)(CO)$_3$(bpy)] indicates that the unusually high frequency of the equatorial ν(CO) A″-like vibration in the NCS complex is caused by the strong vibrational coupling of the ν(NC) vibration with the two symmetrical ν(CO) vibrations.

Excited-State Character. Mixing between MLCT and LLCT characters in low-lying electronic transitions and excited states has been directly demonstrated herein for the first time. This was made possible by using the [Re(NCS)(CO)$_3$(N,N)] complexes, where the effects of electronic excitation on *both* the CO *and* NCS ligands can be followed by TRIR and/or resonance Raman.

The agreement of calculated electronic transition energies, oscillator strengths, and excited-state IR spectra with the experimental results is much better than that reported before for similar low-valent Ru^{II}, Re^{I}, or Mn^{I} carbonyl−diimine complexes with electron-rich ligands, such as halides.[41,43−45,89,90] This was accomplished by including the solvent in the calculations, proper choice of the functional (PBE1PBE), and optimizing the excited-state structures at the TD-DFT level, whereby all contributing one-electron excitations are included in the excited-state description. The transition energies are not underestimated and the LLCT contributions exaggerated as was the case of previous DFT and TD-DFT calculations of similar complexes.

The good agreement between experimental and TD-DFT calculated ground- and excited-state spectra implies that TD-DFT also provides a good description of low-lying electronic transitions and triplet excited states. The two lowest states a^3A'' and a^3A' were calculated so close in energy that it cannot be a priori decided which state is the lowest at actual experimental conditions. The much better correspondence with the experi-

TABLE 7: Wavenumbers (cm^{-1}) of Ground-State and a^{3}A′ Excited-State Vibrations of [Re(NCS)(CO)$_3$(N,N)] Measured and Calculated in a MeCN Solution[a]

[Re(NCS)(CO)$_3$(R-DAB)][b]				[Re(NCS)(CO)$_3$(bpy)]			
GS		a^{3}A′ excited state		GS		a^{3}A′ excited state	
calcd	exptl	calcd	exptl	calcd	exptl	calcd	exptl
1919, A′(2)	1922	1956(CO)	1949	1911, A′(2)	1918	1952 (CO)	1952
1927, A″	1922	1994 (CO; A″)	1994	1914, A″	1918	2010 (NC−CO)	2002
2027, A′(1)	2027	2014 (NC−CO)	2053	2023, A′(1)	2026	2038 (NC+CO)	2041
2101 (NC)	2100	2036 (NC+CO)	∼2068[c]	2104 (NC)	2097	2082 (CO; A″)	2072

[a] Calculation: Turbomole, PBE0, CPCM, values scaled by a factor of 0.9445 to achieve the best correspondence between calculated and experimental values for the ground state. [b] Measured for R = ^{i}Pr, calculated for R = Me. [c] Poorly resolved shoulder.

TABLE 8: TD-DFT Calculated Compositions (in %) of a^{3}A′ Excited-State Vibrations of [Re(NCS)(CO)$_3$(N,N)] Listed in Table 7

N,N	ν (cm^{-1})	symmetry	vibration
bpy	1952	A′	1 ν(NC) + 29 ν(CO$_{eq}^1$) + 29 ν(CO$_{eq}^2$) − 41 ν(CO$_{ax}$)
	2010	A′	58 ν(NC) − 6 ν(CO$_{eq}^1$) − 6 ν(CO$_{eq}^2$) − 30 ν(CO$_{ax}$)
	2038	A′	43 ν(NC) + 15 ν(CO$_{eq}^1$) + 15 ν(CO$_{eq}^2$) − 27 ν(CO$_{ax}$)
	2082	A″	43 ν(CO$_{eq}^1$) − 43 ν(CO$_{eq}^2$) + 14 ν(bpy)
Me-DAB	1956	A′	28 ν(CO$_{eq}^1$) + 28 ν(CO$_{eq}^2$) − 44 ν(CO$_{ax}$)
	1994	A″	48 ν(CO$_{eq}^1$) − 48 ν(CO$_{eq}^2$) + 4 ν(Me-DAB)
	2014	A′	20 ν(NC) − 17 ν(CO$_{eq}^1$) − 17 ν(CO$_{eq}^2$) − 45 ν(CO$_{ax}$)
	2036	A′	81 ν(NC) + 5 ν(CO$_{eq}^1$) + 5 ν(CO$_{eq}^2$) − 9 ν(CO$_{ax}$)

TABLE 9: Wavenumbers (cm^{-1}) of Ground-State and a^{3}A″ Excited-State ν(CO) Vibrations of [Re(Cl)(CO)$_3$(bpy)] Measured in CH_2Cl_2 and Calculated in a MeCN Solution[a]

ground state			a^{3}A″ excited state		
Turbomole	G03	exptl[b]	Turbomole	G03	exptl[b]
1904, A′(2)	1899, A′(2)	1899	1936, A″	1952, A″	1957
1920, A″	1916, A″	1921	1961, A′(2)	1988, A′(2)	1987
2020, A′(1)	2035, A′(1)	2024	2049, A′(1)	2047, A′(1)	2064

[a] Calculation: Turbomole, Gaussian 03, B3-LYP, CPCM calculated values scaled by a factor of 0.963 to achieve the best correspondence between calculated and experimental values for the ground state. [b] From ref 81.

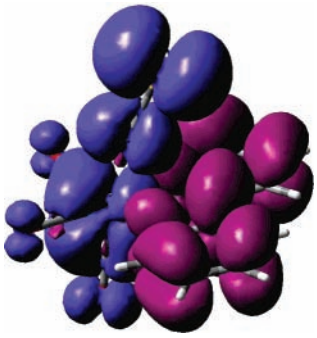

Figure 9. Change of electron density distribution upon the a^{1}A′ → a^{3}A′ electronic transition of [Re(NCS)(CO)$_3$(bpy)]. Blue and violet colors correspond to a decrease and increase of electron density, respectively. Calculated by TD-DFT G03/PBE1PBE/CPCM for MeCN solution.

mental IR spectrum allows us to assign the lowest state as a^{3}A′, of a LLCT/MLCT character. On an orbital level, the LLCT/MLCT mixing can be traced to the principal depopulated orbital, that is HOMO−1, shown in Figure 3. This orbital is delocalized over the Re atom and NCS and CO ligands, Tables 2 and 3. It is π-antibonding with respect to the C≡O and Re−N(CS) bonds and π-bonding with respect to the N═C═S and Re−C bonds. However, it is more rigorous to describe electronic transitions by changes of the electron density upon excitation. Figure 9 clearly shows that the electron density in the a^{3}A′ state is transferred from the Re atom and the NCS and CO ligands to the π* system of bpy. The largest depopulation occurs at Re and NCS, accounting for the MLCT and LLCT contributions, respectively. It should be noted, however, that using the LLCT and MLCT labels and talking about mixed LLCT/MLCT electronic transitions and excited states is tributary to the classical, rather localized, view of charge-transfer transitions. In fact, Figure 9 suggests that the a^{3}A′ excited state can be viewed as delocalized, the electron density being excited from the π system of the entire Re(NCS)(CO)$_3$ moiety.

This description of the a^{3}A′ excited state accounts well for the empirical assignment of the TRIR spectra. Electronic excitation decreases the C≡O π-antibonding and N═C═S π-bonding electron density, shifting the ν(CO) and ν(NC) bands to higher and lower wavenumbers, respectively. TD-DFT analysis, however, indicates that the actual situation is more complicated, revealing that the ν(CO) and ν(NC) vibrations become highly coupled in the excited state. This is quite understandable, given that they involve atoms of comparable masses which are shifted by excitation to very similar frequencies. The coupling is mediated by the electronic "hole" in the excited state that is delocalized over the whole Re(NCS)(CO)$_3$ moiety. This vibrational coupling may account for the relatively small intensity of the 2030 and 2098 cm^{-1} peaks in the resonance Raman spectra. The CO and NC bonds are shortened and lengthened, respectively, upon excitation. Their contributions to the total change of the respective normal coordinates partly cancel each other. The total distortions upon excitation are relatively small, giving rise to only weak resonance Raman enhancements.[75]

The other low-lying triplet is a^{3}A″. It originates in predominantly LLCT/MLCT excitation, together with a smaller contribution from a bpy-localized $\pi \rightarrow \pi^*$ excitation, see Figure 10. The ν(CO) wavenumbers were calculated at a lower wavenumber than in the ground state, in sharp contrast with the experiment. This is probably caused[85] by the $\pi \rightarrow \pi^*$(bpy) contribution to the a^{3}A″ state.

It is also interesting to compare [Re(NCS)(CO)$_3$(N,N)] with other NCS complexes. Thiocyanide is used as an ancillary ligand in Ru(II)−polypyridine sensitizers of Grätzel cells. TD-DFT calculations[61,91] as well as TRIR spectra[92] indicate an involvement of the NCS ligands in the low-lying electronic transitions and excited states. The two ν(NC) bands of the sensitizer [Ru(4,4′-COOH-bpy)$_2$(NCS)$_2$] shift downward upon excitation from 2115 and 2140 cm^{-1} to 2040 and 2075 cm^{-1}, that is by

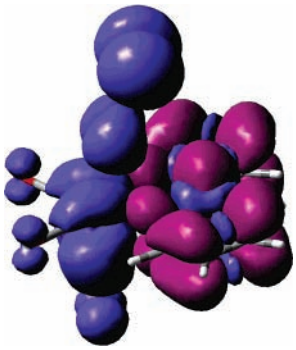

Figure 10. Change of electron density distribution upon the $a^1A' \rightarrow a^3A''$ electronic transition of [Re(NCS)(CO)$_3$(bpy)]. Blue and violet colors correspond to a decrease and increase of electron density, respectively. Calculated by TD-DFT G03/PBE1PBE/CPCM for MeCN solution.

70 cm^{-1} on average.[92] Obviously, the excited state also has a mixed NCS → bpy/Ru → bpy LLCT/MLCT character, similar to that discussed above for Re. Alternatively, it can be viewed as a delocalized CT excitation which originates in the whole Ru(NCS)$_2$ moiety. Another NCS complex whose excited states were studied[93] by time-resolved IR spectroscopy is $Cp_2Ti(NCS)_2$. Its lowest excited state was assigned as NCS → Ti LMCT.[93] The, rather low, shift of the ν(NC) vibrations (−19 cm^{-1}) was attributed[93] to delocalization of the LLCT transition over the two NCS ligands. The mostly NCS π nonbonding character of the HOMO and possible involvement of Cp electron density in the transition can also diminish the ν(NC) IR shift upon electronic excitation of $Cp_2Ti(NCS)_2$.

Conclusions

The lowest allowed electronic transitions and excited states of *fac*-[Re(NCS)(CO)$_3$(N,N)] (N,N = 2,2′-bipyridine (bpy), di-^{i}Pr-*N*,*N*′-1,4-diazabutadiene (^{i}Pr-DAB)) were identified as charge-transfer excitations of electron density from the whole Re(NCS)(CO)$_3$ moiety to the π^* system of the α-diimine ligand N,N. Such excited states can be described as mixed NCS → N,N/Re → N,N LLCT/MLCT. Experimentally, this type of CT transition is manifested (i) by upward and downward shifts of ν(CO) and ν(NC) vibrations upon excitation, respectively, (ii) resonance enhancement of Raman ν(NC) and A′(1) ν(CO) bands, and (iii) a moderate solvatochromism of the electronic absorption band. [Re(NCS)(CO)$_3$(bpy)] has two close-lying emissive ^{3}LLCT/MLCT states, which become equilibrated at room temperature with a common 23 ns lifetime. The lowest excited state of [Re(NCS)(CO)$_3$(^{i}Pr-DAB)] is also ^{3}LLCT/MLCT in character. It is nonemissive and short-lived (∼625 ps).

The right choice of the functional and inclusion of the solvent are the prerequisites for realistic TD-DFT calculations of charge transfer electronic transitions of low-valent metals. Optimization of excited-state structures at a TD-DFT level is possible even for relatively large organometallic compounds. It significantly improves the description of excited states and allows us to interpret emission and excited-state vibrational spectra.

Acknowledgment. We thank EPSRC National Crystallography Service (Southampton) for X-ray data collection on [Re(NCS)(CO)$_3$(bpy)]. EPSRC, COST D14 European collaboration program and Ministry of Education of the Czech Republic (1P04OCD14.20 and OC D14.20) are thanked for funding this research. Taasje Mahabiersing (University of Amsterdam) is acknowledged for measuring the resonance Raman spectra in the KNO_3 pellet. Mr. Jan Sýkora (J. Heyrovský Institute) and Dr. Martin Michl (Czech Technical University, Department of Quantum Electronics) are thanked for their help with the TCSPC experiments.

Supporting Information Available: A figure showing the asymmetric unit of the crystal structure of [Re(NCS)(CO)$_3$(bpy)], tables summarizing DFT G03/B3LYP calculated one-electron energies and compositions of selected highest occupied and lowest unoccupied molecular orbitals of [Re(NCS)(CO)$_3$(bpy)] and [Re(NCS)(CO)$_3$(Me-DAB)], crystal data, bond lengths and angles, structure refinement, atomic coordinates, displacement parameters and hydrogen coordinates of [Re(NCS)(CO)$_3$(bpy)] and [Re(NCS)(CO)$_3$(^{i}Pr-DAB)]. This material is available free of charge via the Internet at http://pubs.acs.org.

References and Notes

(1) Sun, S.-S.; Lees, A. J.; Zavalij, P. Y. *Inorg. Chem.* **2003**, *42*, 3445−3453.
(2) Lo, K. K.-W.; Hui, W.-K.; Ng, D. C.-M.; Cheung, K.-K. *Inorg. Chem.* **2002**, *41*, 40−46.
(3) Yam, V. W.-W.; Lo, K. K.-W.; Cheung, K.-K.; Kong, R. Y.-C. *J. Chem. Soc., Chem. Commun.* **1995**, 1191−1193.
(4) Yam, V. W.-W.; Wong, K. M.-C.; Lee, V. W.-M.; Lo, K. K.-W.; Cheung, K.-K. *Organometallics* **1995**, *14*, 4034.
(5) Guo, X.-Q.; Castellano, F. N.; Li, L.; Lakowicz, J. R. *Anal. Chem.* **1998**, *70*, 632−637.
(6) Oriskovich, T. A.; White, P. S.; Thorp, H. H. *Inorg. Chem.* **1995**, *34*, 1629−1631.
(7) Crane, B. R.; Di Bilio, A. J.; Winkler, J. R.; Gray, H. B. *J. Am. Chem. Soc.* **2001**, *123*, 11623−11631.
(8) Connick, W. B.; Di Bilio, A. J.; Hill, M. G.; Winkler, J. R.; Gray, H. B. *Inorg. Chim. Acta* **1995**, *240*, 169−173.
(9) Di Bilio, A. J.; Crane, B. R.; Wehbi, W. A.; Kiser, C. N.; Abu-Omar, M. M.; Carlos, R. M.; Richards, J. H.; Winkler, J. R.; Gray, H. B. *J. Am. Chem. Soc.* **2001**, *123*, 3181−3182.
(10) Winkler, J. R.; Di Bilio, A. J.; Farrow, N. A.; Richards, J. H.; Gray, H. B. *Pure Appl. Chem.* **1999**, *71*, 1753−1764.
(11) Miller, J. E.; Gradinaru, C.; Crane, B. R.; Di Bilio, A. J.; Wehbi, W. A.; Un, S.; Winkler, J. R.; Gray, H. B. *J. Am. Chem. Soc.* **2003**, *125*, 14220−14221.
(12) Stufkens, D. J.; Vlček, A., Jr. *Coord. Chem. Rev.* **1998**, *177*, 127−179.
(13) Stufkens, D. J. *Comments Inorg. Chem.* **1992**, *13*, 359−385.
(14) Chen, P.; Mecklenburg, S. L.; Meyer, T. J. *J. Phys. Chem.* **1993**, *97*, 13126−13131.
(15) Wang, Y.; Hauser, B. T.; Rooney, M. M.; Burton, R. D.; Schanze, K. S. *J. Am. Chem. Soc.* **1993**, *115*, 5675−5683.
(16) Chen, P.; Westmoreland, T. D.; Danielson, E.; Schanze, K. S.; Anthon, D.; Neveux, P. E., Jr.; Meyer, T. J. *Inorg. Chem.* **1987**, *26*, 1116−1126.
(17) Chen, P.; Duesing, R.; Graff, D. K.; Meyer, T. J. *J. Phys. Chem.* **1991**, *95*, 5850−5858.
(18) Trammell, S.; Goodson, P. A.; Sullivan, B. P. *Inorg. Chem.* **1996**, *35*, 1421−1422.
(19) Chen, P.; Danielson, E.; Meyer, T. J. *J. Phys. Chem.* **1988**, *92*, 3708−3711.
(20) Schoonover, J. R.; Chen, P.; Bates, W. D.; Dyer, R. B.; Meyer, T. J. *Inorg. Chem.* **1994**, *33*, 793−797.
(21) Schoonover, J. R.; Strouse, G. F.; Chen, P.; Bates, W. D.; Meyer, T. J. *Inorg. Chem.* **1993**, *32*, 2618−2619.
(22) Liard, D. J.; Busby, M.; Farrell, I. R.; Matousek, P.; Towrie, M.; Vlček, A., Jr. *J. Phys. Chem. A* **2004**, *108*, 556−567.
(23) Cabana, L. A.; Schanze, K. S. *Adv. Chem. Ser.* **1990**, *226*, 101−124.
(24) Lucia, L. A.; Wang, Y.; Nafisi, K.; Netzel, T. L.; Schanze, K. S. *J. Phys. Chem.* **1995**, *99*, 11801−11804.
(25) Wang, Y.; Lucia, L. A.; Schanze, K. S. *J. Phys. Chem.* **1995**, *99*, 1961−1968.
(26) Wang, Y.; Schanze, K. S. *J. Phys. Chem.* **1996**, *100*, 5408−5419.
(27) Westmoreland, T. D.; Le Bozec, H.; Murray, R. W.; Meyer, T. J. *J. Am. Chem. Soc.* **1983**, *105*, 5952−5954.
(28) Chen, P.; Curry, M.; Meyer, T. J. *Inorg. Chem.* **1989**, *28*, 2271−2280.
(29) Liard, D. J.; Kleverlaan, C. J.; Vlček, A., Jr. *Inorg. Chem.* **2003**, *42*, 7995−8002.
(30) Liard, D. J.; Vlček, A., Jr. *Inorg. Chem.* **2000**, *39*, 485−490.

(31) Yam, V. W.-W.; Lau, V. C.-Y.; Wu, L.-X. *J. Chem. Soc., Dalton Trans.* **1998**, 1461−1468.
(32) Sun, S.-S.; Lees, A. J. *Organometallics* **2002**, *21*, 39−49.
(33) Lewis, J. D.; Perutz, R. N.; Moore, J. N. *Chem. Commun.* **2000**, 1865−1866.
(34) Rossenaar, B. D.; Kleverlaan, C. J.; van de Ven, M. C. E.; Stufkens, D. J.; Vlček, A., Jr. *Chem. Eur. J.* **1996**, *2*, 228−237.
(35) Rossenaar, B. D.; George, M. W.; Johnson, F. P. A.; Stufkens, D. J.; Turner, J. J.; Vlček, A., Jr. *J. Am. Chem. Soc.* **1995**, *117*, 11582−11583.
(36) Kleverlaan, C. J.; Stufkens, D. J.; Clark, I. P.; George, M. W.; Turner, J. J.; Martino, D. M.; van Willigen, H.; Vlček, A., Jr. *J. Am. Chem. Soc.* **1998**, *120*, 10871−10879.
(37) Stor, G. J.; Stufkens, D. J.; Oskam, A. *Inorg. Chem.* **1992**, *31*, 1318−1319.
(38) Rossenaar, B. D.; Stufkens, D. J.; Vlček, A., Jr. *Inorg. Chem.* **1996**, *35*, 2902−2909.
(39) Nieuwenhuis, H. A.; Stufkens, D. J.; McNicholl, R.-A.; Al-Obaidi, A. H. R.; Coates, C. G.; Bell, S. E. J.; McGarvey, J. J.; Westwell, J.; George, M. W.; Turner, J. J. *J. Am. Chem. Soc.* **1995**, *117*, 5579−5585.
(40) Nieuwenhuis, H. A.; Stufkens, D. J.; Oskam, A. *Inorg. Chem.* **1994**, *33*, 3212−3217.
(41) Stor, G. J.; Stufkens, D. J.; Vernooijs, P.; Baerends, E. J.; Fraanje, J.; Goubitz, K. *Inorg. Chem.* **1995**, *34*, 1588−1594.
(42) Rosa, A.; Ricciardi, G.; Baerends, E. J.; Stufkens, D. J. *J. Phys. Chem.* **1996**, *100*, 15346−15357.
(43) Turki, M.; Daniel, C.; Záliš, S.; Vlček, A., Jr.; van Slageren, J.; Stufkens, D. J. *J. Am. Chem. Soc.* **2001**, *123*, 11431−11440.
(44) Záliš, S.; Ben Amor, N.; Daniel, C. *Inorg. Chem.* **2004**, *43*, 7978−7985.
(45) Gabrielsson, A.; Záliš, S.; Matousek, P.; Towrie, M.; Vlček, A., Jr. *Inorg. Chem.* **2004**, *43*, 7380−7388.
(46) Hino, J. K.; Della Ciana, L.; Dressick, W. J.; Sullivan, B. P. *Inorg. Chem.* **1992**, *31*, 1072−1080.
(47) Staal, L. H.; Oskam, A.; Vrieze, K. *J. Organomet. Chem.* **1979**, *170*, 235−245.
(48) Sheldrick, G. M. *SHELX97*, Program for crystal structure determination and refinement; University of Göttingen: Göttingen, Germany, 1998.
(49) Matousek, P.; Towrie, M.; Stanley, A.; Parker, A. W. *Appl. Spectrosc.* **1999**, *53*, 1485−1489.
(50) Matousek, P.; Towrie, M.; Ma, C.; Kwok, W. M.; Phillips, D.; Toner, W. T.; Parker, A. W. *J. Raman Spectroc.* **2001**, *32*, 983−988.
(51) Towrie, M.; Grills, D. C.; Dyer, J.; Weinstein, J. A.; Matousek, P.; Barton, R.; Bailey, P. D.; Subramaniam, N.; Kwok, W. M.; Ma, C. S.; Phillips, D.; Parker, A. W.; George, M. W. *Appl. Spectrosc.* **2003**, *57*, 367−380.
(52) Vlček, A., Jr.; Farrell, I. R.; Liard, D. J.; Matousek, P.; Towrie, M.; Parker, A. W.; Grills, D. C.; George, M. W. *J. Chem. Soc., Dalton Trans.* **2002**, 701−712.
(53) Matousek, P.; Hester, R. E.; Moore, J. N.; Parker, A. W.; Phillips, D.; Toner, W. T.; Towrie, M.; Turcu, I. C. E.; Umapathy, S. *Meas. Sci. Technol.* **1993**, *4*, 1090−1095.
(54) Frisch, M. J.; Trucks, G. W.; Schlegel, H. B.; Scuseria, G. E.; Robb, M. A.; Cheeseman, J. R.; Montgomery, J. A., Jr.; Vreven, T.; Kudin, K. N.; Burant, J. C.; Millam, J. M.; Iyengar, S. S.; Tomasi, J.; Barone, V.; Mennucci, B.; Cossi, M.; Scalmani, G.; Rega, N.; Petersson, G. A.; Nakatsuji, H.; Hada, M.; Ehara, M.; Toyota, K.; Fukuda, R.; Hasegawa, J.; Ishida, M.; Nakajima, T.; Honda, Y.; Kitao, O.; Nakai, H.; Klene, M.; Li, X.; Knox, J. E.; Hratchian, H. P.; Cross, J. B.; Bakken, V.; Adamo, C.; Jaramillo, J.; Gomperts, R.; Stratmann, R. E.; Yazyev, O.; Austin, A. J.; Cammi, R.; Pomelli, C.; Ochterski, J. W.; Ayala, P. Y.; Morokuma, K.; Voth, G. A.; Salvador, P.; Dannenberg, J. J.; Zakrzewski, V. G.; Dapprich, S.; Daniels, A. D.; Strain, M. C.; Farkas, O.; Malick, D. K.; Rabuck, A. D.; Raghavachari, K.; Foresman, J. B.; Ortiz, J. V.; Cui, Q.; Baboul, A. G.; Clifford, S.; Cioslowski, J.; Stefanov, B. B.; Liu, G.; Liashenko, A.; Piskorz, P.; Komaromi, I.; Martin, R. L.; Fox, D. J.; Keith, T.; Al-Laham, M. A.; Peng, C. Y.; Nanayakkara, A.; Challacombe, M.; Gill, P. M. W.; Johnson, B.; Chen, W.; Wong, M. W.; Gonzalez, C.; Pople, J. A. *Gaussian 03*, Revision C.02; Gaussian, Inc.: Wallingford, CT, 2004.
(55) Ahlrichs, R.; Bär, M.; Häser, M.; Horn, H.; Kölmel, C. *Chem. Phys. Lett.* **1989**, *162*, 165−169.
(56) Ahlrichs, R.; Bär, M.; Baron, H. P.; Bauernschmitt, R.; Böcker, S.; Deglmann, P.; Ehrig, M.; Eichkorn, K.; Elliott, S.; Furche, F.; Haase, F.; Häser, M.; Horn, H.; Hättig, C.; Huber, C.; Huniar, U.; Kattannek, M.; Köhn, A.; Kölmel, C.; Kollwitz, M.; May, K.; Ochsenfeld, C.; Öhm, H.; Patzelt, H.; Rubner, O.; Schäfer, A.; Schneider, U.; Sierka, M.; Treutler, O.; Unterreiner, B.; von Arnim, M.; Weigend, F.; Weis, P.; Weiss, H. *TURBOMOLE V5-7*; Quantum Chemistry Group, University of Karlsruhe: Karlsruhe, Germany, 2004.
(57) Furche, F.; Ahlrichs, R. *J. Chem. Phys.* **2002**, *117*, 7433−7447.
(58) Klamt, A.; Jones, V. *J. Chem. Phys.* **1996**, *105*, 9972.
(59) Cossi, M.; Rega, N.; Scalmani, G.; Barone, V. *J. Comput. Chem.* **2003**, *24*, 669.
(60) O'Boyle, N. M.; Vos, J. G. *GaussSum 0.8*; Dublin City University: Dublin, Ireland, 2004.
(61) Monat, J. E.; Rodriguez, J. H.; McCusker, J. K. *J. Phys. Chem. A* **2002**, *106*, 7399−7406.
(62) Záliš, S.; Vlček, A., Jr. *J. Phys. Chem. A* **2005**, *109*, 2991−2992.
(63) Hariharan, P. C.; Pople, J. A. *Theo. Chim. Acta* **1973**, *28*, 213.
(64) Andrae, D.; Häussermann, U.; Dolg, M.; Stoll, H.; Preuss, H. *Theor. Chim. Acta* **1990**, *77*, 123−141.
(65) Woon, D. E.; Dunning, T. H., Jr. *J. Chem. Phys.* **1993**, *98*, 1358.
(66) Stephens, P. J.; Devlin, F. J.; Cabalowski, C. F.; Frisch, M. J. *J. Phys. Chem.* **1994**, *98*, 11623.
(67) Perdew, J. P.; Burke, K.; Ernzerhof, M. *Phys. Rev. Lett.* **1996**, *77*, 3865.
(68) Slageren, J.; Stufkens, D. J.; Záliš, S.; Klein, A. *J. Chem. Soc., Dalton Trans.* **2002**, 218.
(69) Busby, M.; Liard, D. J.; Motevalli, M.; Toms, H.; Vlček, A., Jr. *Inorg. Chim. Acta* **2004**, *357*, 167−176.
(70) Kaim, W.; Kohlmann, S.; Ernst, S.; Olbrich-Deussner, B.; Bessenbacher, C.; Schultz, A. *J. Organomet. Chem.* **1987**, *321*, 215−226.
(71) Stufkens, D. J. *Coord. Chem. Rev.* **1990**, *104*, 39−112.
(72) Nakamoto, K. *Infrared and Raman Spectra of Inorganic and Coordination Compounds. Part B*, 5th ed.; J. Wiley & Sons: New York, 1997.
(73) Smothers, W. K.; Wrighton, M. S. *J. Am. Chem. Soc.* **1983**, *105*, 1067−1069.
(74) van Slageren, J.; Klein, A.; Záliš, S.; Stufkens, D. J. *Coord. Chem. Rev.* **2001**, *219*−*221*, 937−955.
(75) Gamelin, D. R.; George, M. W.; Glyn, P.; Grevels, F.-W.; Johnson, F. P. A.; Klotzbücher, W.; Morrison, S. L.; Russell, G.; Schaffner, K.; Turner, J. J. *Inorg. Chem.* **1994**, *33*, 3246−3250.
(76) Geoffroy, G. L.; Wrighton, M. S. *Organometallic Photochemistry*; Academic Press: New York, 1979.
(77) Lees, A. J. *Chem. Rev.* **1987**, *87*, 711−743.
(78) Chen, P.; Meyer, T. J. *Chem. Rev.* **1998**, *98*, 1439−1477.
(79) Liard, D. J.; Busby, M.; Matousek, P.; Towrie, M.; Vlček, A., Jr. *J. Phys. Chem. A* **2004**, *108*, 2363−2369.
(80) Asbury, J. B.; Wang, Y.; Lian, T. *Bull. Chem. Soc. Jpn.* **2002**, *75*, 973−983.
(81) George, M. W.; Johnson, F. P. A.; Westwell, J. R.; Hodges, P. M.; Turner, J. J. *J. Chem. Soc., Dalton Trans.* **1993**, 2977−2979.
(82) George, M. W.; Turner, J. J. *Coord. Chem. Rev.* **1998**, *177*, 201−217.
(83) Schoonover, J. R.; Strouse, G. F.; Omberg, K. M.; Dyer, R. B. *Comments Inorg. Chem.* **1996**, *18*, 165−188.
(84) Schoonover, J. R.; Strouse, G. F. *Chem. Rev.* **1998**, *98*, 1335−1355.
(85) Dattelbaum, D. M.; Omberg, K. M.; Hay, P. J.; Gebhart, N. L.; Martin, R. L.; Schoonover, J. R.; Meyer, T. J. *J. Phys. Phem. A* **2004**, *108*, 3527−3536.
(86) Dattelbaum, D. M.; Omberg, K. M.; Schoonover, J. R.; Martin, R. L.; Meyer, T. J. *Inorg. Chem.* **2002**, *41*, 6071−6079.
(87) Dattelbaum, D. M.; Martin, R. L.; Schoonover, J. R.; Meyer, T. J. *J. Phys. Chem. A* **2004**, *108*, 3518−3526.
(88) TRIR spectra of [Re(NCS)(CO)$_3$(^{i}Pr-DAB)] display bands at 1946, 1988, 2043, and 2060 cm^{-1} in THF and at 1951, 1989, 2048, and 2063 cm^{-1} in CH_2Cl_2.
(89) Yang, L.; Ren, A.-M.; Feng, J. K.; Liu, X.-J.; Ma, Y.-G.; Zhang, M.; Liu, X.-D.; Shen, J.-C.; Zhang, H.-X. *J. Phys. Chem. A* **2004**, *108*, 6797−6808.
(90) Rosa, A.; Ricciardi, G.; Baerends, E. J.; Stufkens, D. J. *Inorg. Chem.* **1998**, *37*, 6244−6245.
(91) Guillemoles, J.-F.; Barone, V.; Joubert, L.; Adamo, C. *J. Phys. Chem. A* **2002**, *106*, 11354−11360.
(92) Asbury, J. B.; Ellingson, R. J.; Ghosh, H. N.; Ferrere, S.; Nozik, A. J.; Lian, T. *J. Phys. Chem. B* **1999**, *103*, 3110−3119.
(93) Patrick, E. L.; Ray, C. J.; Meyer, G. D.; Ortiz, T. P.; Marshall, J. A.; Brozik, J. A.; Summers, M. A.; Kenney, J. W., III *J. Am. Chem. Soc.* **2003**, *125*, 5461−5470.